Discussion Paper No.310

Stability Switching Curves in a Lotka-Volterra Competition System with Two Delays

Akio Matsumoto
Chuo University

Ferenc Szidarovszky
Corvinus University

March 2019

INSTITUTE OF ECONOMIC RESEARCH
Chuo University
Tokyo, Japan

Stability Switching Curves in a Lotka-Volterra Competition System with Two Delays*

Akio Matsumoto† Ferenc Szidarovszky‡

Abstract

In this study, a Lotka-Volterra competition model with two discrete delays is considered. First we investigate stability conditions of the no-delay model for a positive steady state by analyzing the associated characteristic equation. Second, we establish the stability switching conditions of the delay model under which stability of the model is switched to instability and *vice versa*. Finally, some numerical simulations are performed to confirm the theoretical results such as Hopf bifurcations. However they do not predict the birth of chaotic dynamics and the existence of multistability.

Keywords: Lotka-Volterra system, Competition system, Multiple delays, Hopf bifurcation, Stabilliy loss and gain

*The first author highly acknowledges the financial supports from the Japan Society for the Promotion of Science (Grant-in-Aid for Scientific Research (C) 16K03556) and Chuo University (Grant for Special Research). The usual disclaimers apply.

†Professor, Department of Economics, Chuo University, 742-1, Higashi-Nakano, Hachioji, Tokyo, 192-0393, Japan; akiom@tamacc.chuo-u.ac.jp

‡Professor, Department of Mathematics, Corvinus University, Budapest, Fövám tér 8, 1093, Hungary; szidarka@gmail.com

1 Introduction

In this study, we examine a competitive Lotka-Volterra system (LV system henceforth) with two discrete delays in population biology. It is shown first that the stability conditions in terms of stability switching curves can be rigorously determined and second that the system can generate a wide variety of dynamics ranging from simple dynamics involving limit cycles to complex dynamics involving chaotic behavior when its positive steady state loses stability.

A delay in the LV system has a long history. It is often observed that the population growth of various species depend on the past history of their own as well as that of their competitors. To reflect such history, delays are incorporated into the population dynamic systems. The delays have been thought to have a destabilizing influence. Hatchinson's equation is the prototype model embodying the instabilizing delay phenomenon and is described by the logistic equation with one delay. Since the logistic equation without delays is asymptotically stable, there is a counterplay between a stabilizing negative feedback and the destabilizing influence in the delay equation. May (1973) deals with this phenomenon in the delay predator-prey framework and obtains the instability result. Since then, there have been an enormous amount of works on delay dynamics in the literature. This study follows the same direction and further considers a generalized two species LV competitive system with multiple delays that can be expressed as follows:

$$\begin{aligned} \dot{x}(t) &= x(t)\left[\varepsilon_1 - a_{11}x(t-\tau_{11}) - a_{12}y(t-\tau_{12})\right], \\ \dot{y}(t) &= y(t)\left[\varepsilon_2 - a_{21}x(t-\tau_{21}) - a_{22}y(t-\tau_{22})\right], \end{aligned} \tag{1}$$

where $x(t)$ and $y(t)$ are the population densities of two competing species at time t, $\varepsilon_1 > 0$ and $\varepsilon_2 > 0$ denote the intrinsic growth rates, $\tau_{ij} \geq 0$ and α_{ij} for $i, j = 1, 2,\ i \neq j$ are time delays and positive parameters. Usually $a_{ii} > 0$ is assumed under which the growth follows the logistic equation in the absence of competitors. The interactions between two species are classified into three forms depending on the sign of a_{ij}. They are actually called *competitive* if $a_{ij} > 0$, *cooperative* if $a_{ij} < 0$, and *predator-prey* if $a_{ij} > 0$ and $a_{ji} < 0$ where the predator has a negative coefficient and the prey a positive one. We focus on the competitive system and thus assume that the coefficients are all positive. Further, the coefficients a_{ii} and a_{jj} are called the crowding coefficients of two species measuring the strength of intra-competition within the species and the coefficients a_{ij} and a_{ji} are called the competitive coefficients measuring the strengths of the inter-competitions between the species. The delay τ_{ij} is called the hunting delay while the delay τ_{ii} is the feedback delay to the growth of the species itself and gauges a maturation time.

Over the past few decades, a considerable number of studies have been made on stability of the LV competition system. Those studies may be divided into two groups. One is to study the global stability of the model by constructing appropriate Lyapunov functions. Zhen and Ma (2002) provide sufficient conditions for local and global stability of system (1) with four delays by means

of Lyapunov factions. Saito (2002) presents the necessary and sufficient conditions for the symmetric system (1) with $\alpha_{11} = \alpha_{22} = \alpha$ and $\alpha_{12} = \alpha_{21} = \beta$ by using Lyapunov functions. The other is to focus on linear stability of the corresponding linearized system of (1) and to investigate the location of the solutions in the complex plane. Shibata and Saito (1980) examine system (1) with $\tau_{12} = \tau_{21} = 0$ and numerically exhibit the emergence of complex dynamics as well as simple dynamics. On the other hand, Song et al. (2004) investigate system (1) with $\tau_{11} = \tau_{22} = 0$ and show that a positive steady state is locally asymptotically stable for any value of $\tau = \tau_{12} + \tau_{21} > 0$. These works imply that the hunting delays are harmless and the maturation delays could be a source of instability. Zhang et al. (2009) study the occurrence of Hopf bifurcation and present the stability of limit cycles bifurcating from the Hopf bifurcation in system (1) when $\tau_{11} = \tau_{22} = \tau_{12} = \tau_{21} = \tau > 0$. Zhang (2012) is concerned with system (1) with $\tau_{ii} = \tau$ and $\tau_{ij} > 0$ and obtains conditions under which periodic solutions bifurcate from the positive steady state. Our study is closely related to Zhang et al. (2009) and Zhang (2012). The similarity is that we study the LV competition system (1) with multiple delays and the dissimilarity is that the different roles of two distinct delays are considered by taking into account the notion that the own feedback delay to the growth is different than the cross feedback delay of the competitors. It is to be noticed that although their models have multiple delays, they eventually make some simplifications transforming their models to essentially a one-delay model.

The rest of the study is organized as follows. Section 2 reduces system (1) to an analytically manageable LV competition system with two distinct delays. Section 3 reviews a one-delay LV competition system. Section 4, the main part of this study, derives the stability switching curve that divides the region of the two delays into a stability and instability subregions. Section 5 performs some numerical simulations to visualize the theoretical results obtained previously. Finally, Section 6 concludes this study.

2 Lotka-Volterra Competition Model

First of all, we assume $\tau_{11} = \tau_{21} = \tau_x$, $\tau_{22} = \tau_{12} = \tau_y$ and $\tau_x \neq \tau_y$ in (1) and reduce it to the following Lotka-Volterra competition system with two delays,

$$\begin{aligned} \dot{x}(t) &= x(t)\left[\varepsilon_1 - a_{11}x(t-\tau_x) - a_{12}y(t-\tau_y)\right] \\ \dot{y}(t) &= y(t)\left[\varepsilon_2 - a_{21}x(t-\tau_x) - a_{22}y(t-\tau_y)\right] \end{aligned} \tag{2}$$

where the parameter specification implies that only matured species can hunt their competitors.[1] A stationary state of system (2) satisfies $\dot{x}(t) = \dot{y}(t) = 0$ for

[1] Xu et al (2011) consider a similar model in the predator-prey framework.

any $t \geq 0$ and is expressed by

$$\begin{aligned} x^e &= \frac{\varepsilon_1 a_{22} - \varepsilon_2 a_{12}}{a_{11}a_{22} - a_{12}a_{21}}, \\ y^e &= \frac{\varepsilon_2 a_{11} - \varepsilon_1 a_{21}}{a_{11}a_{22} - a_{12}a_{21}}. \end{aligned} \tag{3}$$

Both of x^e and y^e are positive if the following conditions are satisfied, which can be mentioned as the intra-competition dominates the inter-competition,

Assumption 1. $\dfrac{a_{11}}{a_{21}} > \dfrac{\varepsilon_1}{\varepsilon_2} > \dfrac{a_{12}}{a_{22}}$.

To consider local stability of the stationary state, we linearize system (2) to have the homogenous correspondence,

$$\begin{aligned} \dot{x}(t) &= -\alpha_x x(t-\tau_x) - \beta_x y(t-\tau_y) \\ \dot{y}(t) &= -\beta_y x(t-\tau_x) - \alpha_y y(t-\tau_y) \end{aligned} \tag{4}$$

where the new or reduced coefficients are defined as

$$\alpha_x = a_{11}x^*,\ \beta_x = a_{12}x^* \text{ and } \beta_y = a_{21}y^*,\ \alpha_y = a_{22}y^*. \tag{5}$$

With the exponential solutions, $x(t) = e^{\lambda t}u$ and $y(t) = e^{\lambda t}v$ with $u \neq 0$ and $v \neq 0$, the characteristic equation of system (4) is

$$\det \begin{pmatrix} \lambda + \alpha_x e^{-\lambda\tau_x} & \beta_x e^{-\lambda\tau_y} \\ \beta_y e^{-\lambda\tau_x} & \lambda + \alpha_y e^{-\lambda\tau_y} \end{pmatrix} = 0$$

or expanding the determinant, we have

$$P_0(\lambda) + P_1(\lambda)e^{-\lambda\tau_x} + P_2(\lambda)e^{-\lambda\tau_y} + P_3(\lambda)e^{-\lambda(\tau_x+\tau_y)} = 0 \tag{6}$$

where

$$P_0(\lambda) = \lambda^2,\ P_1(\lambda) = \alpha_x\lambda,\ P_2(\lambda) = \alpha_y\lambda,\ P_3(\lambda) = \alpha_x\alpha_y - \beta_x\beta_y.$$

The stability of the stationary state of system (2) depends on the locations of the roots of the characteristic equation (6) on the complex plane. Although it is well known, we establish the stability of the LV system with no delays, $\tau_x = \tau_y = 0$, as a benchmark. In particular, equation (6) becomes

$$\lambda^2 + (\alpha_x + \alpha_y)\lambda + \left(\alpha_x\alpha_y - \beta_x\beta_y\right) = 0. \tag{7}$$

Since $\alpha_x + \alpha_y > 0$ and

$$\alpha_x\alpha_y - \beta_x\beta_y = (a_{11}a_{22} - a_{12}a_{21})\,x^*y^* > 0$$

by Assumption 1 and the discriminant is positive, the characteristic roots are real and negative, implying local stability.

Theorem 1 *Given Assumption 1, the positive stationary point* (x^e, y^e) *of system* (2) *with* $\tau_x = \tau_y = 0$ *is locally asymptotically stable.*

3 One-Delay Model

We briefly review the results obtained in a one-delay LV competition model in which $\tau_x = \tau_y = \tau > 0$ is assumed. This is essentially the same as Zhang et al. (2009). The corresponding characteristic equation is

$$\lambda^2 + (\alpha_x + \alpha_y)\,\lambda e^{-\lambda\tau} + \left(\alpha_x\alpha_y - \beta_x\beta_y\right) e^{-2\lambda\tau} = 0$$

or multiplying both sides by $e^{\lambda\tau}$ renders it to

$$\lambda^2 e^{\lambda\tau} + (\alpha_x + \alpha_y)\,\lambda + \left(\alpha_x\alpha_y - \beta_x\beta_y\right) e^{-\lambda\tau} = 0. \tag{8}$$

Suppose that $\lambda = i\omega$ with $\omega > 0$ is a root of (8) for some τ. This solution is substituted into (8) to obtain the following forms of the real and imaginary parts

$$\begin{gathered}\left[\omega^2 - \left(\alpha_x\alpha_y - \beta_x\beta_y\right)\right]\cos\omega\tau = 0,\\ -\left[\omega^2 + \left(\alpha_x\alpha_y - \beta_x\beta_y\right)\right]\sin\omega\tau + (\alpha_x + \alpha_y)\,\omega = 0.\end{gathered} \tag{9}$$

If we assume $\omega^2 = \left(\alpha_x\alpha_y - \beta_x\beta_y\right)$ from the first equation of (9), then the second equation implies

$$\sin\omega\tau = \frac{\alpha_x + \alpha_y}{2\sqrt{\alpha_x\alpha_y - \beta_x\beta_y}} > 1$$

where the last inequality is due to

$$(\alpha_x + \alpha_y)^2 - 4\left(\alpha_x\alpha_y - \beta_x\beta_y\right) > 0 \text{ and } \omega = \sqrt{\alpha_x\alpha_y - \beta_x\beta_y} > 0$$

and contradicts $|\sin\omega\tau| \le 1$. Hence we have, from the first equation,

$$\cos\omega\tau = 0 \text{ and } \sin\omega\tau = \pm 1.$$

When $\sin\omega\tau = +1$, the second equation,

$$\omega^2 - (\alpha_x + \alpha_y)\,\omega + \left(\alpha_x\alpha_y - \beta_x\beta_y\right) = 0,$$

yields two positive solutions ,

$$\omega_\pm = \frac{1}{2}\left\{\alpha_x + \alpha_y \pm \sqrt{(\alpha_x + \alpha_y)^2 - 4\left(\alpha_x\alpha_y - \beta_x\beta_y\right)}\right\}$$

with $0 < \omega_- < \omega_+$. When $\sin\omega\tau = -1$, then the second equation is reduced to

$$\omega^2 + (\alpha_x + \alpha_y)\,\omega + \left(\alpha_x\alpha_y - \beta_x\beta_y\right) = 0.$$

Both roots are real and negative. Hence we have two critical values of the delay

$$0 < \tau_{+,n} = \frac{1}{\omega_+}\left(\frac{\pi}{2} + 2n\pi\right) \text{ and } \tau_{-,n} = \frac{1}{\omega_-}\left(\frac{\pi}{2} + 2n\pi\right) \text{ for } n = 0, 1, 2, \ldots . \tag{10}$$

We can think of the roots of (8) as continuous functions in terms of the delay τ and then determine the sign of the derivative of $\mathrm{Re}\left[d\lambda(\tau)/d\tau\right]$ at the point where $\lambda(\tau)$ is purely imaginary. Assuming $\alpha_x = \alpha_y = \alpha$ for analytical simplicity and then differentiating the following form of the characteristic equation,

$$\lambda^2 + 2\alpha\lambda e^{-\lambda\tau} + \left(\alpha^2 - \beta_x\beta_y\right) e^{-2\lambda\tau} = 0 \tag{11}$$

yield

$$\left\{\left(\lambda + \alpha e^{-\lambda\tau}\right) - \tau\left[\alpha\lambda e^{-\lambda\tau} + \left(\alpha^2 - \beta_x\beta_y\right) e^{-2\lambda\tau}\right]\right\}\frac{d\lambda}{d\tau} = \lambda\left[\alpha\lambda e^{-\lambda\tau} + \left(\alpha^2 - \beta_x\beta_y\right) e^{-2\lambda\tau}\right].$$

For convenience, we study $\left(d\lambda/d\tau\right)^{-1}$ instead of $d\lambda/d\tau$

$$\begin{aligned}\left(\frac{d\lambda}{d\tau}\right)^{-1} &= \frac{\lambda + \alpha e^{-\lambda\tau}}{\lambda\left[\alpha\lambda e^{-\lambda\tau} + \left(\alpha^2 - \beta_x\beta_y\right) e^{-2\lambda\tau}\right]} - \frac{\tau}{\lambda} \\ &= -\frac{1}{\lambda^2} - \frac{\tau}{\lambda}\end{aligned}$$

where equation (11) is used in the last step. Inserting $\lambda = i\omega$ where $\omega = \omega_+$ or $\omega = \omega_-$ and taking the real part present

$$\mathrm{Re}\left[\left(\frac{d\lambda}{d\tau}\right)^{-1}_{\lambda=i\omega}\right] = \mathrm{Re}\left[-\frac{1}{(i\omega)^2} - \frac{\tau}{i\omega}\right] = \frac{1}{\omega^2} > 0.$$

The last inequality implies that the crossing of the imaginary axis is from left to right as τ is increasing and the stability of the steady state is lost. Stability cannot be regained science at each critical value at least one pair of eigenvalues changes real part from negative to positive. Summarizing these results present the following.

Theorem 2 *(Theorem 2.5 of Zhang et al. (2009)) The steady state of system* (2) *with $\tau_x = \tau_y = \tau$ is locally asymptotically stable for $\tau < \tau_{+,0}$, loses stability at $\tau = \tau_{+,0}$ and bifurcates to a limit cycle for $\tau > \tau_{+,0}$ where $\tau_{+,0}$ is the smallest critical value of τ and defined as*

$$\tau_{+,0} = \frac{\pi}{2\omega_+}.$$

4 Two Delay Model

We now suppose $\tau_x > 0$ and $\tau_y > 0$ and consider how the positive delays affect stability of system (2). We can see that $\lambda = 0$ does not solve the characteristic equation and thus find all purely complex roots. To this end, we assume that $\lambda = i\omega$ with $\omega > 0$. Substituting it into the characteristic equation gives

$$P_0(i\omega) + P_1(i\omega)e^{-i\omega\tau_x} + P_2(i\omega)e^{-i\omega\tau_y} + P_3(i\omega)e^{-i\omega(\tau_x+\tau_y)} = 0 \tag{12}$$

with

$$P_0(i\omega) = -\omega^2,\ P_1(i\omega) = i\alpha_x\omega,\ P_2(i\omega) = i\alpha_y\omega,\ P_3(i\omega) = \alpha_x\alpha_y - \beta_x\beta_y. \quad (13)$$

Applying the method developed by Matsumoto and Szidarovszky (2018) that is based on Lin and Wang (2012), we derive the set of points (τ_x, τ_y) for which the delay system (2) has purely complex roots. Equation (12) is written as

$$P_0(i\omega) + P_1(i\omega)e^{-i\omega\tau_x} + \left[P_2(i\omega) + P_3(i\omega)e^{-i\omega\tau_x}\right] e^{-i\omega\tau_y} = 0. \quad (14)$$

Since $\left|e^{-i\omega\tau_y}\right| = 1$, equation (14) has solution for τ_x if and only if

$$\left|P_0(i\omega) + P_1(i\omega)e^{-i\omega\tau_x}\right| = \left|P_2(i\omega) + P_3(i\omega)e^{-i\omega\tau_x}\right|$$

or squaring both sides presents the equivalent form,

$$\left(P_0(i\omega) + P_1(i\omega)e^{-i\omega\tau_x}\right)\left(\bar{P}_0(i\omega) + \bar{P}_1(i\omega)e^{i\omega\tau_x}\right)$$

$$= \left(P_2(i\omega) + P_3(i\omega)e^{-i\omega\tau_x}\right)\left(\bar{P}_2(i\omega) + \bar{P}_3(i\omega)e^{i\omega\tau_x}\right)$$

where over-bar indicates complex conjugate. After some calculations, the last equation can be reduced to

$$|P_0|^2 + |P_1|^2 - |P_2|^2 - |P_0|^2 = 2A_x(\omega)\cos\omega\tau_x - 2B_x(\omega)\sin\omega\tau_x. \quad (15)$$

where the argument of P_i is omitted for the sake of notational simplicity and

$$A_x(\omega) = \mathrm{Re}\left(P_2\bar{P}_3 - P_0\bar{P}_1\right) \text{ and } B_x(\omega) = \mathrm{Im}\left(P_2\bar{P}_3 - P_0\bar{P}_1\right).$$

Using $P_k(i\omega)$ for $k = 0, 1, 2, 3$ in (13), we obtain

$$P_2\bar{P}_3 - P_0\bar{P}_1 = i\omega\left[\alpha_y\left(\alpha_x\alpha_y - \beta_x\beta_y\right) - \alpha_x\omega^2\right]$$

which implies

$$A_x(\omega) = 0$$

and

$$B_x(\omega) = \alpha_x\omega\left[\frac{\alpha_y}{\alpha_x}\left(\alpha_x\alpha_y - \beta_x\beta_y\right) - \omega^2\right]. \quad (16)$$

Thus equation (15) is reduced to

$$|P_0|^2 + |P_1|^2 - |P_2|^2 - |P_3|^2 = -2B_x(\omega)\sin\omega\tau_x \quad (17)$$

To find an appropriate pair of τ_x and τ_y satisfying equation (14), we first examine the case of $B_x(\omega) = 0$ and then proceed to the case of $B_x(\omega) \neq 0$.

4.1 Case 1: $B_x(\omega) = 0$

Let ω_x be a positive solution of $B_x(\omega) = 0$ that makes the right hand side of (17) zero,

$$\omega_x^2 = \frac{\alpha_y}{\alpha_x}\left(\alpha_x\alpha_y - \beta_x\beta_y\right) > 0$$

where the inequality is due to Assumption 1. Also let $f(\omega)$ be the left hand side of equation (17). Substituting $P_k(i\omega)$ for $k = 0, 1, 2, 3$ into $f(\omega)$ and rearranging terms, we obtain

$$f(\omega) = \omega^4 + (\alpha_x^2 - \alpha_y^2)\omega^2 - \left(\alpha_x\alpha_y - \beta_x\beta_y\right)^2.$$

Solving $f(\omega) = 0$ yields two solutions,

$$\omega_\pm^2 = \frac{1}{2}\left[-(\alpha_x^2 - \alpha_y^2) \pm \sqrt{(\alpha_x^2 - \alpha_y^2)^2 + 4\left(\alpha_x\alpha_y - \beta_x\beta_y\right)^2}\right].$$

Comparing ω_x^2 with ω_+^2 reveals that both solutions are identical if $\alpha_x = \alpha_y$. There is no solution of τ_x for equation (17) if $\alpha_x \neq \alpha_y$ because $f(\omega_x) \neq 0$ and $B_x(\omega_+) \neq 0$. Only for the sake of analytical simplicity, we make a little bit stronger conditions;

Assumption 2. $\alpha_x = \alpha_y = \alpha$ and $\beta_x = \beta_y = \beta$.

Under Assumption 2, we have

$$\omega_x^2 = \omega_+^2 = \alpha^2 - \beta^2 > 0.$$

Let ω^* be the positive solution of the last equation,

$$\omega^* \,(= \omega_x = \omega_+) = \sqrt{\alpha^2 - \beta^2} > 0.$$

With this identical assumption, $f(\omega) = 0$ and $B_x(\omega) = 0$ for $\omega = \omega^*$, that is, equation (17) holds. The corresponding values of τ_y can be obtained from equation (14)

$$e^{-i\omega\tau_y} = -\frac{P_0(i\omega) + P_1(i\omega)e^{-i\omega\tau_x}}{P_2(i\omega) + P_3(i\omega)e^{-i\omega\tau_x}}. \tag{18}$$

An explicit form of τ_y against $\tau_x \geq 0$ is derived as follows. Using Euler's formula, equation (18) can be rewritten as

$$\cos\omega\tau_y - i\sin\omega\tau_y = -\frac{-\omega^2 + \alpha\omega\sin\omega\tau_x + i\alpha\omega\cos\omega\tau_x}{\left(\alpha^2 - \beta^2\right)\cos\omega\tau_x + i\left[\alpha\omega - \left(\alpha^2 - \beta^2\right)\sin\omega\tau_x\right]}. \tag{19}$$

For simplification of the right hand side, we multiply the denominator and the numerator of (19) by the conjugate of the denominator. Then the denominator becomes

$$D_x = \left[\left(\alpha^2 - \beta^2\right)\cos\omega\tau_x\right]^2 + \left[\alpha\omega - \left(\alpha^2 - \beta^2\right)\sin\omega\tau_x\right]^2 > 0.$$

The new numerator can be denoted by $M_x + iN_x$ where the real part is

$$M_x = \beta^2\omega^2 \cos\omega\tau_x \tag{20}$$

and the imaginary part is

$$N_x = \alpha\omega\left(\alpha^2 - \beta^2\right) + \alpha\omega^3 - \omega^2\left(2\alpha^2 - \beta^2\right)\sin\omega\tau_x. \tag{21}$$

Replacing ω with ω^* and comparing the left hand side of (19) with $-M_x/D_x + i\left(N_x/D_x\right)$ yield

$$\cos\omega^*\tau_y = -\frac{M_x}{D_x} \text{ and } \sin\omega^*\tau_y = \frac{N_x}{D_x}.$$

For further development, we need to specify parameter values so that we take the following specification adopted by Shibata and Saito (1980);

Specification I: $a_{11} = a_{22} = 2,\ a_{12} = a_{21} = 1$ and $\varepsilon_1 = \varepsilon_2 = 2$.

Using (3) and (5) with this specification, we have the following values for the reduced parameters,

$$\alpha_x = \alpha_y = \alpha = \frac{4}{3},\ \beta_x = \beta_y = \beta = \frac{2}{3} \text{ and } (\omega^*)^2 = \frac{4}{3}.$$

The graphs of $-M_x/D_x$ and N_x/D_x are illustrated as red and blue curves for $\tau_x \in (0, 2\pi/\omega^*)$ in Figure 1. The red curve intersects the horizontal axis twice at which $M_x = 0$ or $\cos\omega^*\tau_x = 0$ from (20). Hence we have $\omega^*\tau_x = \pi/2$ at point B and $\omega^*\tau_x = 3\pi/2$ at point D,

$$\tau_x^B = \frac{\pi}{2\omega^*} \simeq 1.36 \text{ and } \tau_x^D = \frac{3\pi}{2\omega^*} \simeq 4.08.$$

It is also seen that the blue curve intersects the horizontal axis twice at which $N_x = 0$ from (21) or

$$\sin\omega^*\tau_x = \frac{2\alpha\left(\alpha^2 - \beta^2\right)}{\sqrt{\alpha^2 - \beta^2}\left(2\alpha^2 - \beta^2\right)} = \frac{4\sqrt{3}}{7} \simeq 0.9897 < 1.$$

Since points A and C are left, respectively, right to point B and $\sin\omega^*\tau_x$ takes the maximum value $+1$ at point B with $\omega^*\tau_x^B = \pi/2$, we have $\omega^*\tau_x^A < \pi/2$ at point A at which $\cos\omega^*\tau_x^A > 0$ and $\omega^*\tau_x^C > \pi/2$ at point C at which $\cos\omega^*\tau_x^C < 0$. Hence

$$\tau_x^A = \frac{1}{\omega^*}\sin^{-1}\left(\frac{4\sqrt{3}}{7}\right) \simeq 1.24$$

and

$$\tau_x^C = \frac{1}{\omega^*}\left[\pi - \sin^{-1}\left(\frac{4\sqrt{3}}{7}\right)\right] \simeq 1.48.$$

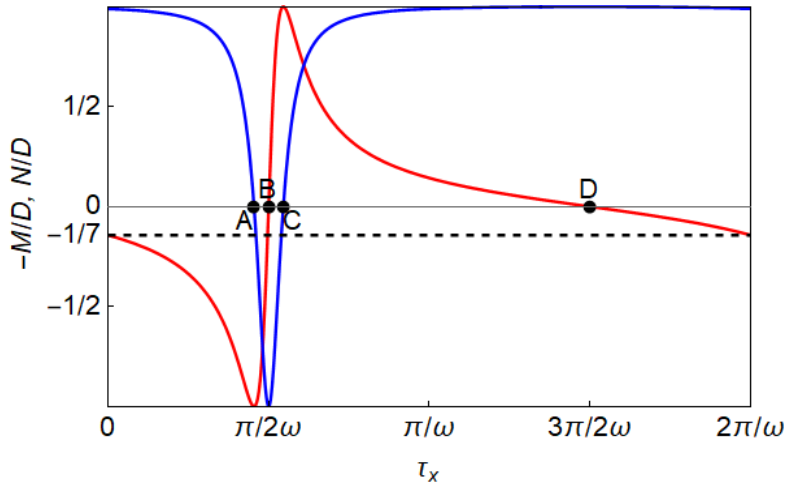

Figure 1. Graphs of M_x/D_x (red) and N_x/D_x (blue).

The interval $[0, 2\pi/\omega^*]$ is divided into five subintervals. In the first subinterval $(0, \tau_x^A)$, it is seen that $\cos\omega^*\tau_y < 0$ and $\sin\omega^*\tau_y > 0$. Hence solving $\cos\omega^*\tau_y = -M_x/D_x$ and $\sin\omega^*\tau_y = N_x/D_x$ for τ_y determines the corresponding values of τ_y satisfying equation (18),

$$\tau_y^c(\tau_x) = \frac{1}{\omega^*}\cos^{-1}\left(-\frac{M_x}{D_x}\right) \text{ and } \tau_y^s(\tau_x) = \frac{1}{\omega^*}\left[\pi - \sin^{-1}\left(\frac{N_x}{D_x}\right)\right] \tag{22}$$

where the superscripts c and s stand for cos and sin, respectively. In the same way, we have $\cos\omega^*\tau_y < 0$ and $\sin\omega^*\tau_y < 0$ for $\tau_x \in \left(\tau_x^A, \tau_x^B\right)$ in which

$$\tau_y^c(\tau_x) = \frac{1}{\omega^*}\left[2\pi - \cos^{-1}\left(-\frac{M_x}{D_x}\right)\right] \text{ and } \tau_y^s(\tau_x) = \frac{1}{\omega^*}\left[\pi - \sin^{-1}\left(\frac{N_x}{D_x}\right)\right]. \tag{23}$$

For $\tau_x \in \left(\tau_x^B, \tau_x^C\right)$, $\cos\omega^*\tau_y > 0$ and $\sin\omega^*\tau_y < 0$ imply

$$\tau_y^c(\tau_x) = \frac{1}{\omega^*}\left[2\pi - \cos^{-1}\left(-\frac{M_x}{D_x}\right)\right] \text{ and } \tau_y^s(\tau_x) = \frac{1}{\omega^*}\left[2\pi + \sin^{-1}\left(\frac{N_x}{D_x}\right)\right]. \tag{24}$$

For $\tau_x \in \left(\tau_x^C, \tau_x^D\right)$, $\cos\omega^*\tau_y > 0$ and $\sin\omega^*\tau_y > 0$ imply

$$\tau_y^c(\tau_x) = \frac{1}{\omega^*}\cos^{-1}\left(-\frac{M_x}{D_x}\right) \text{ and } \tau_y^s(\tau_x) = \frac{1}{\omega^*}\sin^{-1}\left(\frac{N_x}{D_x}\right). \tag{25}$$

Finally, we have $\cos\omega^*\tau_y < 0$ and $\sin\omega^*\tau_y > 0$ for $\tau_x \in \left(\tau_x^D, 2\pi/\omega^*\right)$ as in the first subinterval,

$$\tau_y^c(\tau_x) = \frac{1}{\omega^*}\cos^{-1}\left(-\frac{M_x}{D_x}\right) \text{ and } \tau_y^s(\tau_x) = \frac{1}{\omega^*}\left[\pi - \sin^{-1}\left(\frac{N_x}{D_x}\right)\right]. \tag{26}$$

Since $\tau_y^c(\tau_x) = \tau_y^s(\tau_x)$ holds for $\tau_x \in [0, 2\pi/\omega^*]$, the solution can be denoted by $\tau_y(\tau_x)$.

The locus of $(\tau_x, \tau_y(\tau_x))$ for $\tau_x \in [0, 2\pi/\omega^*]$ constructs the crossing curves in case of $B_x(\omega) = 0$ that are illustrated by two black-red curves in Figure 2. More precisely, the upper convex-shaped curve consists of three segments, the lowest black segment described by (22), the middle red segment by (23) and the highest black segment by (24) whereas the lower concave-shaped curve consists of two segments, the left black segment by (25) and the right red segments by (26). Because of the trigonometric representations, there are infinitely many values of $\tau_y(\tau_x)$, we only represent the smallest solutions. The results obtained so far are summarized as follows:

Theorem 3 *If $B_x(\omega) = 0$ for $\omega = \omega^*$, $\alpha_x = \alpha_y = \alpha$, $\beta_x = \beta_y = \beta$ and $\alpha > \beta$, then the crossing curve is described by the locus of $(\tau_x, \tau_y(\tau_x))$ where*

$$\tau_y(\tau_x) = \frac{1}{\omega^*} \cos^{-1}\left(-\frac{M_x}{D_x}\right) \text{ for } \tau_x \in (0, \tau_x^A) \cup \left(\tau_x^C, \tau_x^D\right) \cup \left(\tau_x^D, 2\pi/\omega^*\right)$$

and

$$\tau_y(\tau_x) = \frac{1}{\omega^*}\left[2\pi - \cos^{-1}\left(-\frac{M_x}{D_x}\right)\right] \text{ for } \tau_x \in \left(\tau_x^A, \tau_x^B\right) \cup \left(\tau_x^B, \tau_x^C\right)$$

where

$$\omega^* = \sqrt{\alpha^2 - \beta^2} > 0.$$

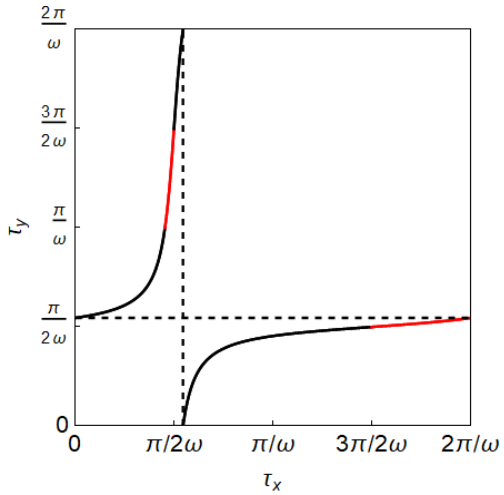

Figure 2. Crossing curves in case of $B_x(\omega) = 0$

4.2 Case 2: $|B_x(\omega)| > 0$

In this section we consider the case of $\omega \neq \omega^*$. We determine values of τ_x satisfying equation (14) in the first half and then values of τ_y in the second half.

Since equation (16) can be rewritten as

$$B_x(\omega) = \alpha_x \omega \left(\omega_x + \omega\right)\left(\omega_x - \omega\right)$$

with

$$\omega_x = \sqrt{\frac{\alpha_y}{\alpha_x}\left(\alpha_x\alpha_y - \beta_x\beta_y\right)},$$

there exists $\varphi_x(\omega)$ such that

$$\varphi_x(\omega) = \arg\left[P_2\bar{P}_3 - P_0\bar{P}_1\right] = \begin{cases} \dfrac{\pi}{2} & \text{if } B_x(\omega) > 0 \text{ or } \omega < \omega_x, \\ \dfrac{3\pi}{2} & \text{if } B_x(\omega) < 0 \text{ or } \omega > \omega_x, \end{cases}$$

implying that

$$\sin\left[\varphi_x(\omega)\right] = \frac{B_x(\omega)}{\sqrt{B_x(\omega)^2}} = 1 \text{ and } \cos\left[\varphi_x(\omega)\right] = \frac{A_x(\omega)}{\sqrt{B_x(\omega)^2}} = 0.$$

Rewriting the first equation as $B_x(\omega) = \sqrt{B_x(\omega)^2}\sin\left[\varphi_x(\omega)\right]$ and applying the addition theorem, equation (17) can be reduced to

$$|P_0|^2 + |P_1|^2 - |P_2|^2 - |P_3|^2 = 2\sqrt{B_x(\omega)^2}\cos\left[\varphi_x(\omega) + \omega\tau_x\right] \tag{27}$$

where the following relation with $\cos\left[\varphi_x(\omega)\right] = 0$ is used,

$$-\sin\left[\varphi_x(\omega)\right]\cos\omega\tau_x = \cos\left[\varphi_x(\omega)\right]\sin\omega\tau_x - \sin\left[\varphi_x(\omega)\right]\cos\omega\tau_x.$$

Rewriting equation (27) presents

$$\frac{|P_0|^2 + |P_1|^2 - |P_2|^2 - |P_3|^2}{2\sqrt{B_x(\omega)^2}} = \cos\left[\varphi_x(\omega) + \omega\tau_x\right] \le 1.$$

Hence a sufficient and necessary condition for the existence of $\tau_x > 0$ satisfying the above equation is

$$\left||P_0|^2 + |P_1|^2 - |P_2|^2 - |P_3|^2\right| \le 2\sqrt{B_x(\omega)^2}$$

or

$$F(\omega) = \left||P_0|^2 + |P_1|^2 - |P_2|^2 - |P_3|^2\right|^2 - 4B_x(\omega)^2 \le 0.$$

Substituting $P_k(i\omega)$ for $k = 0, 1, 2, 3$ in (13) into the right hand side of $F(\omega)$ gives

$$F(\omega) = \omega^8 + a_6\omega^6 + a_4\omega^4 + a_2\omega^2 + a_0 \tag{28}$$

where

$$a_6 = -4(\alpha_x^2 + \alpha_y^2),$$

$$a_4 = (\alpha_x^2 - \alpha_y^2)^2 + 2\left(3\alpha_x\alpha_y + \beta_x\beta_y\right)\left(\alpha_x\alpha_y - \beta_x\beta_y\right),$$

$$a_2 = -2(\alpha_x^2 + \alpha_y^2)\left(\alpha_x\alpha_y - \beta_x\beta_y\right)^2,$$

$$a_0 = \left(\alpha_x\alpha_y - \beta_x\beta_y\right)^4.$$

With $x = \omega^2$, the right hand side of equation (28) can be factorized as

$$x^4 + a_6 x^3 + a_4 x^2 + a_2 x + a_0 = F_1(x) \cdot F_2(x)$$

where $F_1(x)$ and $F_2(x)$ are quadratic in x,

$$F_1(x) = x^2 - \left(\alpha_x^2 + \alpha_y^2 + 2\beta_x\beta_y\right) x + \left(\alpha_x\alpha_y - \beta_x\beta_y\right)^2$$

and

$$F_2(x) = x^2 - \left(\alpha_x^2 + \alpha_y^2 - 2\beta_x\beta_y\right) x + \left(\alpha_x\alpha_y - \beta_x\beta_y\right)^2.$$

Solving $F_1(x) = 0$ gives two real roots,

$$x_1 = \frac{1}{2}\left[\alpha_x^2 + \alpha_y^2 + 2\beta_x\beta_y - (\alpha_x + \alpha_y)\sqrt{(\alpha_x - \alpha_y)^2 + 4\beta_x\beta_y}\right]$$

$$x_2 = \frac{1}{2}\left[\alpha_x^2 + \alpha_y^2 + 2\beta_x\beta_y + (\alpha_x + \alpha_y)\sqrt{(\alpha_x - \alpha_y)^2 + 4\beta_x\beta_y}\right]$$

and solving $F_2(x) = 0$ gives two real roots,

$$x_3 = \frac{1}{2}\left[\alpha_x^2 + \alpha_y^2 - 2\beta_x\beta_y - (\alpha_x - \alpha_y)\sqrt{(\alpha_x + \alpha_y)^2 - 4\beta_x\beta_y}\right]$$

$$x_4 = \frac{1}{2}\left[\alpha_x^2 + \alpha_y^2 - 2\beta_x\beta_y + (\alpha_x - \alpha_y)\sqrt{(\alpha_x + \alpha_y)^2 - 4\beta_x\beta_y}\right]$$

since the discriminant is positive,

$$(\alpha_x + \alpha_y)^2 - 4\beta_x\beta_y = (\alpha_x - \alpha_y)^2 + 4\left(\alpha_x\alpha_y - \beta_x\beta_y\right) > 0.$$

If $\alpha_x = \alpha_y$, then the second term in the last two square brackets are zero, implying that $F_2(x) = 0$ generates equal roots,

$$x_1 < x_2 \text{ and } x_3 = x_4.$$

If $\alpha_x > \alpha_y$, then all roots are real and distinct and it is clear that

$$x_1 < x_2 \text{ and } x_3 < x_4.$$

If the inequality is reversed, then the subscripts of x_3 and x_4 should be interchanged but there is essentially no harm. So we adopt $\alpha_x > \alpha_y$ in the asymmetric case. Further, subtracting $F_1(x)$ from $F_2(x)$ presents

$$F_2(x) - F_1(x) = 4\beta_x\beta_y x > 0 \text{ for } x > 0.$$

This inequality implies the following ordering among real roots if $\alpha_x \geq \alpha_y$,

$$x_1 < x_3 \leq x_4 < x_2.$$

Let ω_i be a positive solution of $x_i = \omega^2$, then

$$0 < \omega_1 < \omega_3 \leq \omega_4 < \omega_2.$$

Therefore we have the interval union $[\omega_1, \omega_3] \cup [\omega_4, \omega_2]$ that is denoted by Ω in which $F(\omega) \leq 0$.

Let us define $\psi_x(\omega)$ by

$$|P_0|^2 + |P_1|^2 - |P_2|^2 - |P_0|^2 = 2\sqrt{B_x(\omega)^2}\cos\left[\psi_x(\omega)\right] \tag{29}$$

or

$$\psi_x(\omega) = \cos^{-1}\left[\frac{|P_0|^2 + |P_1|^2 - |P_2|^2 - |P_3|^2}{2\sqrt{B_x(\omega)^2}}\right].$$

Comparing the right hand side of (27) with that of (29) presents the critical values of delay τ_x,

$$\tau^{\pm}_{x,m}(\omega) = \frac{1}{\omega}\left[\pm\psi_x(\omega) - \varphi_x(\omega) + 2m\pi\right] \text{ for } m = 0, 1, 2, \ldots . \tag{30}$$

To determine the corresponding values of delay τ_y, we return to equation (12) and alternatively put it as

$$P_0(i\omega) + P_2(i\omega)e^{-i\omega\tau_y} + \left[P_1(i\omega) + P_3(i\omega)e^{-i\omega\tau_y}\right]e^{-i\omega\tau_x} = 0. \tag{31}$$

Similarity of (31) to (14) is clear. Hence, in the same way, we can define the critical value of τ_y as

$$\tau^{\pm}_{y,n}(\omega) = \frac{1}{\omega}\left[\pm\psi_y(\omega) - \varphi_y(\omega) + 2n\pi\right] \text{ for } n = 0, 1, 2, \ldots, \tag{32}$$

where

$$\begin{aligned} A_y(\omega) &= \mathrm{Re}\left[P_1\bar{P}_3 - P_0\bar{P}_2\right] = 0, \\ B_y(\omega) &= \mathrm{Im}\left[P_1\bar{P}_3 - P_0\bar{P}_2\right] = \alpha_y\omega\left[\frac{\alpha_x}{\alpha_y}\left(\alpha_x\alpha_y - \beta_x\beta_y\right) - \omega^2\right], \end{aligned}$$

$$\psi_y(\omega) = \cos^{-1}\left[\frac{|P_0|^2 - |P_1|^2 + |P_2|^2 - |P_3|^2}{2\sqrt{B_y(\omega)^2}}\right]$$

and

$$\varphi_y(\omega) = \arg\left[P_1\bar{P}_3 - P_0\bar{P}_2\right] = \begin{cases} \dfrac{\pi}{2} & \text{if } B_y(\omega) > 0 \text{ of } \omega < \omega_y, \\ \dfrac{3\pi}{2} & \text{if } B_y(\omega) < 0 \text{ of } \omega > \omega_y \end{cases}$$

with ω_y being a positive solution of $B_y(\omega) = 0$,

$$\omega_y = \sqrt{\frac{\alpha_x}{\alpha_y}\left(\alpha_x\alpha_y - \beta_x\beta_y\right)}.$$

In case of $B_y(\omega) = 0$, we solve (31) to have

$$e^{-i\omega\tau_x} = -\frac{P_0(i\omega) + P_2(i\omega)e^{-i\omega\tau_y}}{P_1(i\omega) + P_3(i\omega)e^{-i\omega\tau_y}}. \tag{33}$$

Two remarks should be addressed. First, in the same way as to derive $\tau_y(\tau_x)$ from equation (14), we can derive $\tau_x(\tau_y)$ from equation (31) and construct the crossing curve $(\tau_x(\tau_y), \tau_y)$. Second, equations (14) and (31) are different expressions derived from the same characteristic equation (12). As a result the crossing curve $(\tau_x, \tau_y(\tau_x))$ is identical with the crossing curve $(\tau_x(\tau_y), \tau_y)$. To define $\psi_y(\omega)$, we need a condition similar to $F(\omega)$,

$$G(\omega) = \left||P_0|^2 - |P_1|^2 + |P_2|^2 - |P_3|^2\right|^2 - 4B_y(\omega)^2 \leq 0.$$

Since it can be shown that $F(\omega) = G(\omega)$, the solutions of $F(\omega) = 0$ also solve $G(\omega) = 0$, although a solution of $B_x(\omega) = 0$ is different from a solution of $B_y(\omega) = 0$,

$$\omega_x^2 < \omega_y^2 \text{ if } \alpha_x > \alpha_y.$$

In Figure 4(A), the crossing curve under Assumption 2 and Specification 1 is illustrated as an egg-shaped closed curve and the parts of the crossing curve in case of $B_x(\omega) = 0$ are over-illustrated. Under these parameter specification, the blue and red segments are described, respectively, by

$$\left(\tau_{x,0}^+(\omega), \tau_{y,1}^-(\omega)\right) \text{ for } \omega \in [\omega_1, \omega_3]$$

and

$$\left(\tau_{x,1}^-(\omega), \tau_{y,0}^+(\omega)\right) \text{ for } \omega \in [\omega_1, \omega_3]$$

with

$$\varphi_x(\omega) = \varphi_y(\omega) = \frac{\pi}{2}$$

whereas the green and orange curves are described by

$$\left(\tau_{x,1}^+(\omega), \tau_{y,1}^-(\omega)\right) \text{ for } \omega \in [\omega_4, \omega_2]$$

and

$$\left(\tau_{x,1}^-(\omega), \tau_{y,1}^+(\omega)\right) \text{ for } \omega \in [\omega_4, \omega_2]$$

with

$$\varphi_x(\omega) = \varphi_y(\omega) = \frac{3\pi}{2}.$$

At the origin of $\tau_x = \tau_y = 0$, the stationary state is confirmed to be locally asymptotically stable. Hence in Figure 4(A), the region including the origin and being surrounded by the black, orange and blue segments is the stability region. Further its boundary is the stability switching curve on which the real part of an eigenvalues are zero. Equations (30) and (32) indicate that increasing values of m and n increase the values of $\tau_x^{\pm}(\omega)$ and $\tau_y^{\pm}(\omega)$, respectively. Graphically, this implies that increasing value of m shifts the closed curve rightward and

increasing value of n shifts the closed curve upward. Hence, it can be mentioned that m is a horizontal-shift parameter and n is a vertical-shift parameter.

We turn attention to the asymmetric case in which we take the following parameter specification where only the value of a_{22} is increased to 5/2.

Specification II: $a_{11} = 2,\ \alpha_{22} = 5/2,\ a_{12} = \alpha_{21} = 1$ and $\varepsilon_1 = \varepsilon_2 = 2$

It can be checked that given Specification 2, the reduced parameters take the following values,

$$\alpha_x = \frac{3}{2} > \alpha_y = \frac{5}{4},\ \beta_x = \frac{3}{4} \text{ and } \beta_y = \frac{1}{2}.$$

The crossing curves in case of $\alpha_x > \alpha_y$ are illustrated in Figure 4(B). Although $\omega_x < \omega_y$, we have

$$\omega_3 < \omega_x < \omega_y < \omega_4$$

since substituting ω_x and ω_y into $F_2(x)$ yields

$$F_2(\omega_x) = -\frac{(\alpha_x - \alpha_y)^2 \beta_x \beta_y \left(\alpha_x \alpha_y - \beta_x \beta_y\right)}{\alpha_x^2} < 0$$

and

$$F_2(\omega_y) = -\frac{(\alpha_x - \alpha_y)^2 \beta_x \beta_y \left(\alpha_x \alpha_y - \beta_x \beta_y\right)}{\alpha_y^2} < 0.$$

The fact that $F_2(x)$ is quadratic with $F(\omega_3) = F(\omega_4) = 0$ implies the above inequality relation. Hence

$$B_x(\omega) > 0 \text{ and } B_y(\omega) > 0 \text{ for } \omega \in (\omega_1, \omega_3) \text{ implying } \varphi_x(\omega) = \varphi_y(\omega) = \frac{\pi}{2}$$

and

$$B_x(\omega) < 0 \text{ and } B_y(\omega) < 0 \text{ for } \omega \in (\omega_4, \omega_2) \text{ implying } \varphi_x(\omega) = \varphi_y(\omega) = \frac{3\pi}{2}.$$

Applying the same procedure to obtain the egg-shaped crossing curve, we can derive the crossing curve in Figure 4(B) under the following parameter specification. Two notices are given: First, the case of $B_x(\omega) = B_y(\omega) = 0$ does not occur when $\alpha_x > \alpha_y$; second, the shape of the crossing curves are distorted. The stationary state is locally asymptotically stable in the region including the origin and being surrounded by the blue, orange and green curves. The boundary of this region is the stability switching curve in case of $\alpha_x > \alpha_y$.[2] We refer to the two horizontal dotted lines in each figure shortly when we perform numerical simulations. The results obtained so far are summarized as follows:

[2] Interchanging the horizontal and vertical axes gives the stability switching curve for $\alpha_x = 5/4 < \alpha_y = 3/2$, $\beta_x = 1/2$ and $\beta_y = 3/4$.

Theorem 4 *Given Assumption 2 and if* $B_x(\omega) \neq 0$ *and* $B_y(\omega) \neq 0$, *then the pairs of delays obtained from (30) and (32) as*

$$\left\{ \left(\tau^{\pm}_{x,m}(\omega), \tau^{\mp}_{y,n}(\omega) \right) \mid \omega \in \Omega \right\},$$

give the set of all crossing curves on the (τ_x, τ_y) *plane for equations (2).*

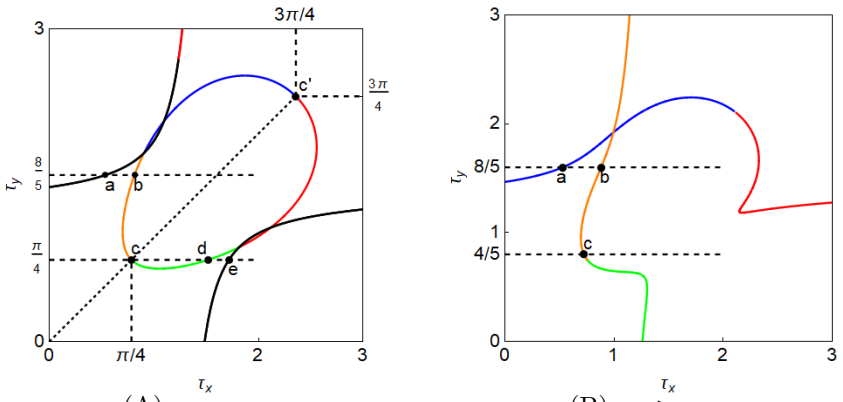

(A) $\alpha_x = \alpha_y$ (B) $\alpha_x > \alpha_y$

Figure 3. Stability switching curves with $B_j(\omega) \neq 0$ for $j = x, y$

5 Numerical Simulations

We numerically confirm the analytical results obtained so far by simulating system (2) with Specification I or II. Initial functions are assumed to be constant,

$$\varphi_x(t) = x^e + x_0 \text{ and } \varphi_y(t) = y^e + y_0 \text{ for } t \leq 0 \tag{34}$$

where x^e and y^e are the steady state obtained in (3), x_0 and y_0 are some constants.

In the first example with $x_0 = y_0 = 0.01$, we perform simulations of the one-delay model discussed in Section 3, that is, (2) with $\tau_x = \tau_y = \tau$, as a special case of the two-delay model. Delay τ is increased along the diagonal of Figure 3(A) that passes through the connecting point of the orange and green segments. According to Theorem 2, the stability is lost at the critical value of the delay that is obtained from (10) with $n = 0$ as

$$\tau_{+,0} = \frac{\pi}{4} \simeq 0.775.$$

Since the point is also on the stability switching curve, the critical value can be obtained from Theorem 6,[3]

$$\tau^{-}_{x,1}(\omega_3) = \tau^{+}_{y,1}(\omega_3) = \frac{\pi}{4} \text{ at point } c.$$

Needless to say, both values are the same and thus denoted as τ_*. Theorem 2 predicts that the steady state is locally asymptotically stable for $\tau < \tau_*$ and loses stability at point c from which a limit cycle emerges and becomes larger as the value of τ increases. More specifically, Figure 4(A) is a bifurcation diagram with respect to τ representing a locus of $(\tau_x, y(t))$ under Specification I.[4] As is seen in Figure 4(A), the lower part of the diagram after the second bifurcation point $\tau^A \simeq 1.057$ is compressed and almost invisible.[5] To avoid this inconvenience, Figure 4(B) reproduces the same diagram in the $(\tau_x, \log x(t))$ plane in which a period-doubling cascade is clearly seen.

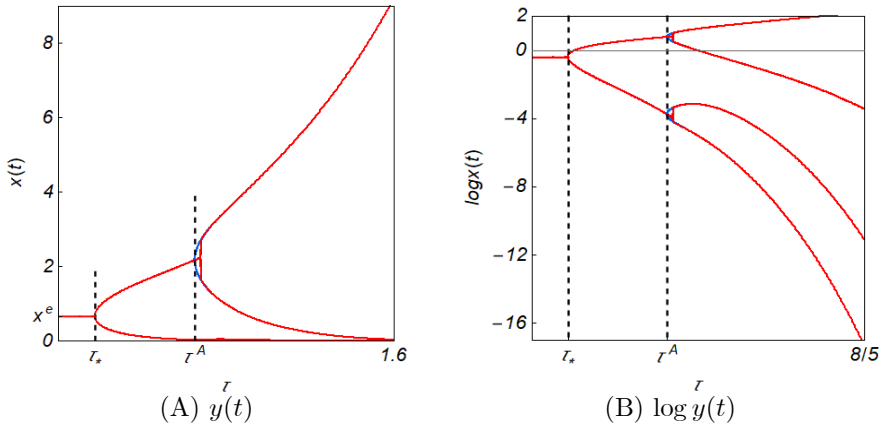

(A) $y(t)$ (B) $\log y(t)$

Figure 4. Bifurcation diagrams of the one-delay model with $\tau_x = \tau_y = \tau$

A close look at these diagrams reveals two points that the analytical results do not refer to: one is that a time trajectory could be negative or its amplitude becomes extremely large, implying loss of biological meaning and the other is the occurrence of multistability over a small interval of τ in which a stable steady

[3] In the same way we have

$$\tau_{-,0} = \frac{3\pi}{4} \simeq 2.36$$

and at point c'

$$\tau^{+}_{x,0}(\omega_4) = \tau^{-}_{y,1}(\omega_4) = \frac{3\pi}{4}.$$

[4] The diagram is constructed in the following procedure. The value of τ is increased from $\pi/4 - 0.1$ to $8/5$ with an increment 0.001. For each value of τ, system runs for $0 \le t \le T = 1000$ and the data for $t \le T - 50$ are discarded to get rid of the initial disturbance. The remaining data are plotted against this τ value. The value of τ is increased and then the same procedured is repeated until τ arrives at $8/5$.

[5] The value of τ^A is a rough estimate.

state and a limit cycle coexist. Figure 5(A) enlarges the vicinity of the second bifurcation point of the diagram of Figure 4(A). For τ in interval $[\tau^m, \tau^M]$ with $\tau^m = 1.05$ and $\tau^M = 1.085$, the blue curve is obtained with different initial functions $\phi_x(t) = x^e + 0.1$ and $\phi_y(t) = y^e + 3$ and the red diagram with (34) is superposed on the blue one. It is seen that both trajectories are identical for $\tau < \tau^A$, the blue curve bifurcates to a periodic cycle for $\tau > \tau^A$ while along the red curve, the steady state is still stable for $\tau > \tau^A$ but to a limited extent, and then jumps to a periodic solution around $\tau = \tau^B \simeq 1.069$. After that, the red curve is again identical with the blue one. We take $\tau = \tau^B$ and obtain the phase diagram in Figure 5(B). The blue curve depicts a periodic solution and takes a two-fold widely extended oval shape. The red curve describes a periodic solution with a very long period. Summarizing the results, the one-delay model most likely generates periodic solutions after loss of stability.

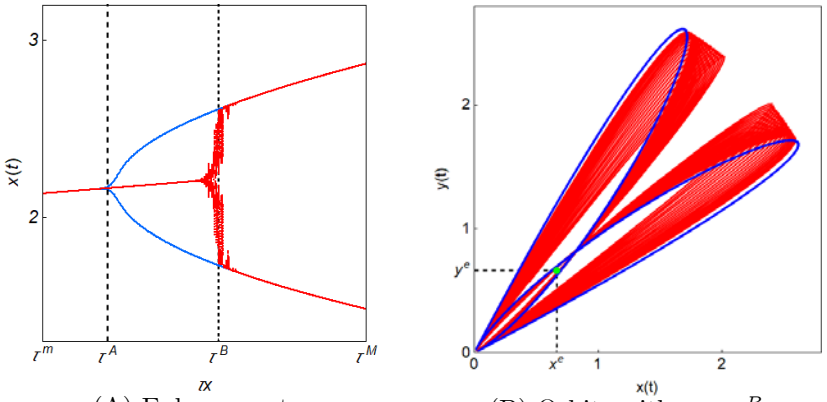

(A) Enlargement (B) Orbits with $\tau = \tau^B$

Figure 5. Multistability over $[\tau^A, \tau^B]$

We now draw attention to the delay effects caused by two positive delays. In the second example, we simulate system (2) with Specification I in the following way. The value of τ_y is fixed at $8/5$ and the value of τ_x is increased from 0 to $8/5$. Applying a similar procedure than in the first example, we have the bifurcation diagram of $x(t)$ with respect to τ_x as illustrated in Figure 6. Graphically τ_x increases along the upper dotted line at $\tau_y = 8/5$ in Figure 3(A) in which the dotted line crosses the stability switching curve twice at point a on the upper black segment and at point b on the orange segment where the abscissas of these points are

$$\tau_x^a \simeq 0.536 \text{ and } \tau_x^b \simeq 0.814.$$

In the interval $[0, \tau_x^a)$, the stationary state is locally unstable because the dotted line is in the unstable region above the black boundary. It is seen in the bifurcation diagram shown in Figure 6(A) that the unstable stationary state is replaced with a limit cycle. Stability is gained in the interval (τ_x^a, τ_x^b) since the dotted line segment ab is in the stable region. At point b, the stationary state

loses stability again and then undergoes a period-doubling bifurcation to complex dynamics involving chaos as τ_x increases and further increasing the values of τ_x induces a period-halving bifurcation. Figure 6(B) plots $(\tau_x, \log x(t))$ in order to clarify dynamic behavior of the lower parts of the bifurcation diagram in the interval $(\tau_x^b, 8/5)$,which is again compressed and thus almost invisible in Figure 6(A). The period-doubling and the period-halving cascades in the lower part are clearly seen in Figure 6(B).

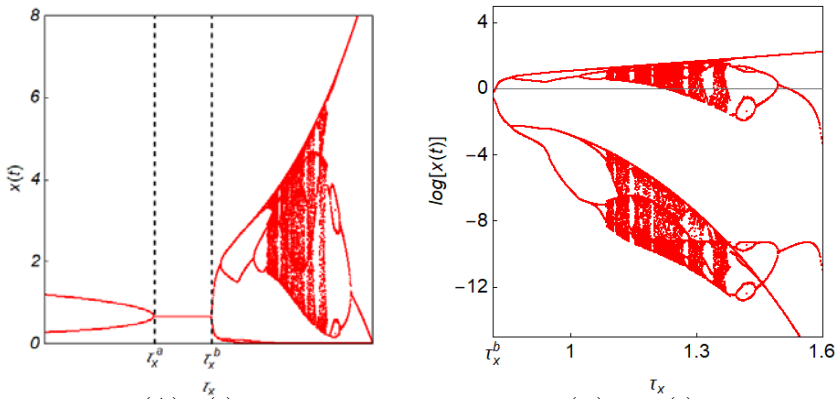

(A) $x(t)$ (B) $logx(t)$

Figure 6. Bifurcation diagrams of $x(t)$ and $\log x(t)$ with respect to τ_x

In the third simulation, the fixed value of τ_y is decreased to $\pi/4$ and τ_x is increased along the lower horizontal dotted line at $\tau_y = \pi/4$ of Figure 3(A). In Figure 3(A), the horizontal line crosses the stability switching curve three times at points c, d and e where the abscissas are

$$\tau_x^c \simeq 0.772,\ \tau_x^d \simeq 1.560 \text{ and } \tau_x^e \simeq 1.726.$$

Multiple stability losses and gains occur in Figure 7(A). The stationary state is stable in the intervals $(0, \tau_x^c)$ and (τ_x^d, τ_x^e). On the other hand, it is unstable in (τ_x^c, τ_x^d) and for $\tau_x > \tau_x^e$, periodic cycles with various periodicity are created. To see what dynamic comes out for $\tau > \tau_x^e$, we take $\tau_x^1 = 1.9$ with $\tau_y = \pi/4$ and perform simulation to obtain the phase diagram shown in Figure 7(B) in which the steeper line is the $\dot{x}(t) = 0$ locus and the flatter line is the $\dot{y}(t) = 0$ locus. As expected, a periodic solution with larger periodicity oscillates around

the steady state S.

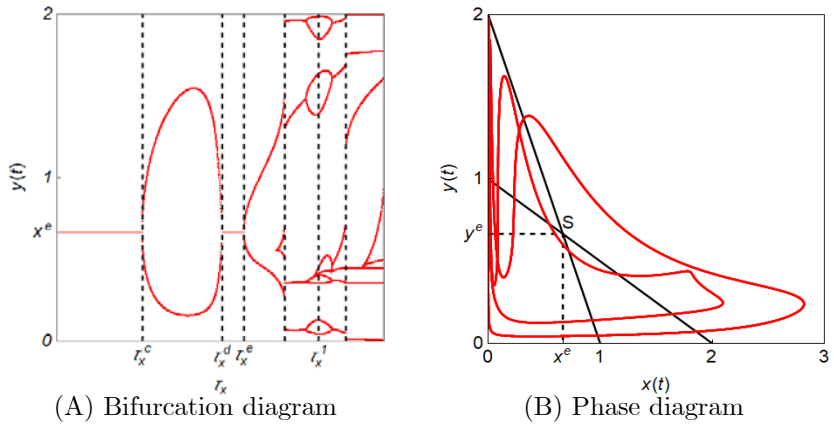

(A) Bifurcation diagram (B) Phase diagram

Figure 7. Birth if varuiys periodic solutions

In the fourth example, we simulate the model with Specification II. The horizontal line at $\tau_y = 8/5$ in Figure 3(B) crosses the stability switching curve twice at point a with $\tau_x^a \simeq 0.331$ and point b with $\tau_x^b \simeq 0.906$. Comparing the resultant bifurcation diagram in Figure 8(A) with that in Figure 6(A) seems to give rise no big qualitative difference. We incline to mention that the differences in parameter specification do not generate any qualitatively different results. However, to look more carefully at the diagrams in a small neighborhood of τ_x^b brings us to find that the diagram makes a jump at $\tau = \tau_x^b$. To see what dynamics emerges there, we enlarge that part and obtain the bifurcation diagram over interval $[\tau_x^b - 0.01, \tau_x^b + 0.01]$ presented in Figure 8(B) in which two occurrences of multistabily are observed. The blue curve has initial functions, $\varphi_x(t) = x^e$ and $\varphi_y(t) = y^e + 3$ whereas the red curve has $\varphi_x(t) = x^e + 0.01$ and $\varphi_y(t) = y^e + 0.01$. In interval $[\tau_x^m, \tau_x^b]$ with $\tau_x^m \simeq 0.9008$, the stable state coexists with a periodic solution. Further, for $\tau_x > \tau_x^b$, the coexistence of periodic cycles with different periodicity is observed, which is similar to that given in Figure 5(A). Notice that the same phenomenon occurs along the lower branch of the bifurcation diagram of Figure 8(B) but is invisible. Under Specification II, numerical considerations confirm the theoretical results and show what the theoretical results do not

predict.

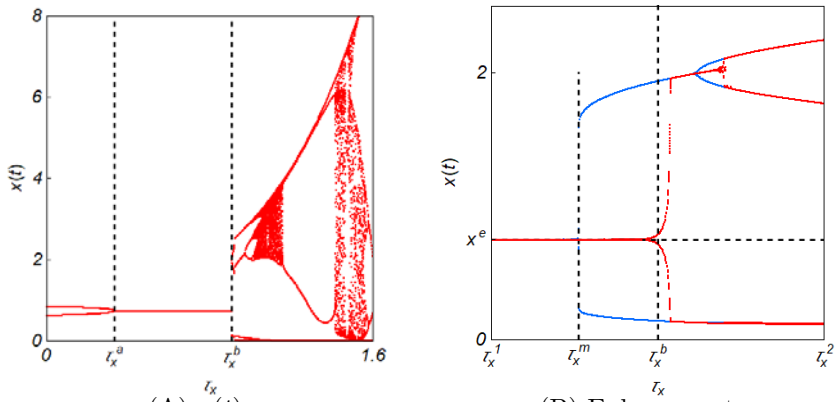

(A) $x(t)$ (B) Enlargement

Figure 8. Bifurcation diagram with $a_{11} < a_{22}$

In the fifth example, we decrease the value of τ_y to $\pi/4$ and simulate the model, increasing the value of τ_x along the lower dotted line of Figure 3(B) from 0 to 2.7. The steady state loses stability when the dotted line crosses the stability switching curve at $\tau_x^c = \pi/4$ and bifurcates to a periodic solution. A two-period cycle emerges for $\tau \in (\tau_x^c, \tau_x^1)$ with $\tau_x^1 \simeq 1.91$ and bifurcates to a periodic cycle with multiple periods for $\tau > \tau_x^1$. The vertical line at $\tau_x^3 \simeq 2.56$ in Figure 9(A) crosses the bifurcation diagrams many times. Accordingly, the closed orbit in Figure 9(B) oscillates around the steady state value of $\log[y(t)]$ many time.

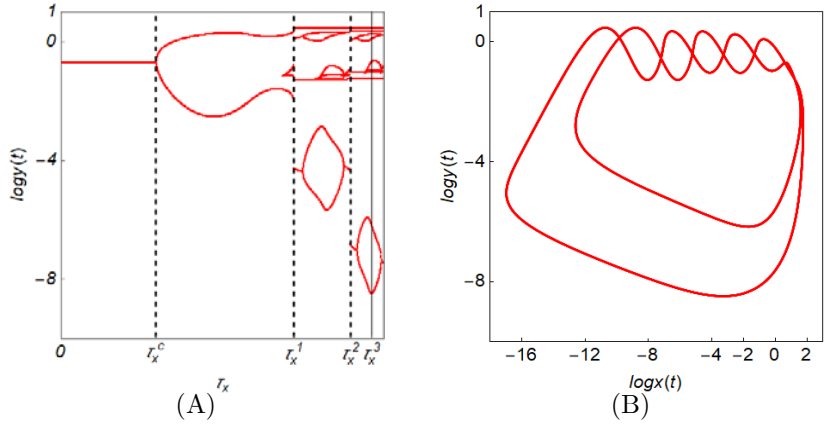

(A) (B)

Figure 9. Bifurcation diagrams

6 Concluding Remarks

In this study, we analytically and numerically investigate a Lotka-Volterra competition system with two delays, a maturation delay and a hunting delay. We first review the well-known results that without delays, two competition species can coexist if the intra-competition dominates the inter-competition. Under this stability condition, we introduce delays to consider how the delays affect the otherwise stable system, to be more specific, to validate whether the delays cause the loss of stability and induces various oscillations. To this end, we study the model in which the length of the maturation delay is identical with that of the identical delay. It is shown that there is a critical value of the delay and the steady state is locally asymptotically stable for a smaller delay, it loses stability at the critical value and it is replaced with a limit cycle through a Hopf bifurcation for a larger delay. For the model with two distinct delays, we establish the analytical formula for constructing the stability switching curve in the delay space, on which stability of the steady state is lost. Lastly we perform simulations to verify what the analytical results predict. In particular, it is demonstrated that the competing system can generate a wide variety of dynamics ranging from periodic solution with various periods to complex dynamics involving chaos. It is further demonstrated what the analytical results do not predict, that is, occurrence of multistability in which the stable steady state coexists with periodic solutions, appearance of chaos via period-doubling bifurcation and disappearance of chaos via period-halving bifurcation.

References

Lin, X. and Wang, E. Stability analysis of delay differential equations with two discrete delays, *Canadian Applied Mathematics Quarterly*, 20, 579-532, 2012.

Matsumoto, A. and Szidarovszky, F., *Dynamic oligopolies with time delays*, Tokyo, Springer-Verlag, 2018.

May, R., Time delay versus stability in population models with two and three trophic levels, *Ecology*, 54, 315-325, 1973.

Shibata, A. and Saito, N., Time delays and chaos in two competing species, *Mathematical Biosciences*, 51, 199-211, 1980.

Saito, Y., The necessary and sufficient condition for global stability of a Lotka-Volterra cooperative or competition system with delays, *Journal of Mathematical Analysis and Applications*, 268, 109-124, 2002.

Song, Y., Han, M. and Pend, Y., Stability and Hopf bifurcations in a competitive Lotka-Volterra system with two delays, *Chaos, Solitions and Fractals*, 22, 1139-1148, 2004.

Xu C., Tang, X., Liao, M and He, X., Bifurcation analysis in a delayed Lotka-Volterra predator-prey model with two delays, *Nonlinear Dynamics*, 66, 169-183, 2011.

Zhang, J. F., Stability and bifurcation periodic solutions in a Lotka-Volterra competition system with multiple delays, *Nonlinear Dynamics*, 70, 849-860, 2012.

Zhang, J., Jin, Z., Yan, J. and Sun, G., Stability and Hopf bifurcation in a delayed competition system, *Nonlinear Analysis*, 70, 658-670, 2009.

Zhen, J. and Ma Z., Stability for a competitive Lotka-Volterra system with delays, *Nonlinear Analysis*, 51, 1131-1142, 2002.